International Journal of Chemical, Materials and Biomolecular Sciences
ISSN: 2415-6620
Vol:9, No:7, 2015

Thermomechanical and Metallurgical Analysis of SMA and GTA Welded Low Carbon Steel Butt Joints

J. Dutta, P. Pranith Kumar Reddy

***Abstract*—**This research paper portrays a comparative analysis of thermomechanical behaviour of Shielded Metal Arc Welding (SMAW) and Gas Tungsten Arc Welding (GTAW) of low carbon steel of AISI 1020 grade butt joints. The thermal history has been obtained by experimental work. We have focused on temperature dependent cooling rate as depicted by Adam's two-dimensional model. The effect of moving point heat source of SMAW and GTAW on mechanical properties has been judged by optical and scanning electron micrographs of different regions in weld joints. The microhardness study has been carried to visualize the joint strength due to formation of different phases.

***Keywords*—**Shielded metal arc welding, gas tungsten arc welding, low carbon steel, microhardness study, thermal history, microscopic morphology.

I. Introduction

LOW carbon steel (mild steel) of grade AISI 1020 experiences a large application in engineering field where application demands for malleability and ductility. In fully heat treated condition, mild steel offers higher ductility which makes it useful in railway coach and wagon factories (different structural parts). Fusion welding of steel joints is very useful due their modification of mechanical properties such as higher hardness, improved tensile strength, decreasing brittleness. Shielded Metal Arc Welding (SMAW) and Gas Tungsten Arc Welding (GTAW) are most common and traditional fusion welding processes. Basically, fusion welding is a process which comprises of rapid heating and cooling cycle. It produces a non-uniform and transient temperature distribution which causes rapid thermal expansion followed by thermal contraction which in turn develops non-homogeneous plastic deformation and thermal stresses in welded joints when it cools down gradually. The thermal cycle appeared in the vicinity of fusion boundary influences the Heat Affected Zone (HAZ) [1]. Thus the impact of thermal cycle and its effect on mechanical and metallurgical parameters must be essential to study to produce and modify the design parameters of weld sections. Rosenthal [2] first developed an effective analytical model for estimating temperature cycle of moving point heat source and its effect on other process variables such as welding velocity, thermal conductivity, specific heat etc. Rosenthal's analytical model assumes localized point heat source and it is not valid for higher temperature due to its several assumptions based on uniform, quasi-steady state process. Pavelic et al. [3] first suggested distributed heat flux and have correlated with Gaussian surface heat flux distribution, experimental as well as analytical by defining molten zone, size, and shape. Tsai and Hou [4] have produced theoretical study of weld pool behaviour based on analytical model of pulsed GTAW. Jones et al. [5] carried out analytical and experimental study of welding parameters of fusion welds. Handful work has been provided by [6] which estimated mathematical modeling of thermal stress in solids in the vicinity of liquid region. Little and Kamtekar [7] analyzed the thermal properties in connection with melting weld efficiency in transient state. One of the best research work (in last two decades) has been represented by [8], [9] who developed analytical model of heat source based on ring temperature distribution and provided an elaborate theoretical study of several process parameters involved in fusion welding process. Zhu and Chao [10] developed FEM code for welding simulation of temperature dependent material properties with detailed non-linear thermomechanical analysis. Cooling rate of different plate thickness has been calculated by [11] with an innovative method. Mousavi and Miresmaeili [12] derived numerical analysis of heat source distribution along with residual stress propagation and have validated with experimental work conducted through GTA welding of AISI 304L steel. Del Coz Diaz [13] investigated comparative study of TIG welding distortions of austenitic and duplex stainless steel by implementing thermograph image analyzer of TIG torch at different positions of weld pool and simulation based work carried out by the application of volumetric heat flux distribution functions. Pathak et al. [14] proposed a new technique on the basis of coupled convection-radiation heat transfer to calculate the rate of heat transfer influenced by temperature cycle from the weld joint during multi-pass arc welding. Ravisankar et al. [15] estimated thermal history based on numerical simulation and experimental work of AISI 304 stainless steel welded joints of GTAW. Alireza et al. [16] carried out computational analysis of the effect of welding parameters on energy consumption in GTA welding process on the basis of conservation of momentum equation along with solid-liquid interface.

The major contribution of researchers in the field of mechanical and metallurgical parameters of steel welded joints influenced by heat source has depicted the glimpse of research work in the area of fusion welding of steel butt joints. Mohandas et al. [17] have portrayed the effect of shielding gas and addition of grain refining elements on the weld zone tensile properties of ferrtic stainless steel (AISI 430) in arc

Jaideep Dutta is with the Department Mechanical Engineering of Manipal University Jaipur, India (e-mail: duttajd1212@gmail.com).

P. Pranith Kumar Reddy is with the Department Mechanical Engineering of Parul Institute of Engineering and Technology, Vadodara, Gujarat, India. (e-mail: pranithkumarash@gmail.com).

welding. Datta et al. [18] presented weldability characteristics of SMAW welded high strength quenched and tempered plates. Ahmet [19] analyzed the effect of hydrogen in argon as shielding gas on GTAW of stainless steel. Bala Srinivasan et al. [20] investigated the microstructure and corrosion behaviour of SMAW joints of low alloy steel in conjunction with austenitic and duplex grade electrodes. A phenomenal research work has been represented by [21] who found out the effect of SMAW and Flux Cored Arc Welding (FCAW) processes on tensile and impact properties of high strength quenched and tempered steel joints. Moeinifar et al. [22] figured out the influence of peak temperature on simulated and real thermal cycles on microstructure and fracture properties of the reheated zones of welded samples. Wichan and Loeshphan [23] studied the effect of welding speed on microstructure, mechanical properties and corrosion analysis of GTA welded AISI 201 sheets.

Motivated by the research work as summarized above, present work has been undertaken to provide a comparative study (both theoretical and experimental) of thermal and mechanical process parameters involved in GTAW and SMAW of AISI 1020 steel butt joints.

II. Theoretical Study

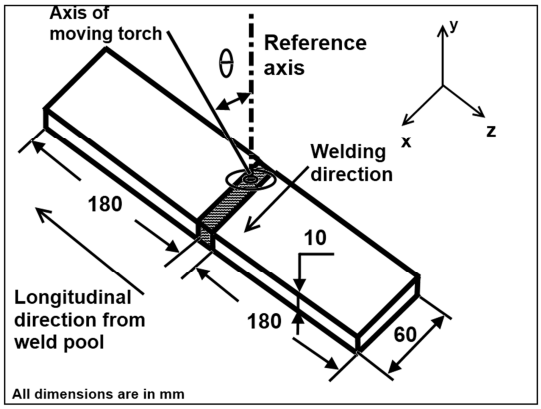

Fig. 1 Schematic diagram of moving point heat source with angular torch heat flux distribution

To evaluate the rate of cooling along the longitudinal direction from the fusion boundary, we have utilized the Adams's 2-D equation [11] for heat flow and it can be mathematically expressed as:

$$\frac{dT}{dt} = 2\pi k\rho C_p \left(\frac{d}{H_{net}}\right)^2 (T_P - T_0)^2 \quad (1)$$

where, 'k' is thermal conductivity, ρ is density of material (solid), C_P is specific heat, 'd' is plate thickness, H_{net} is net heat input (J/mm), T_P is peak temperature at particular location, T_0 is ambient temperature (30°C). Fig. 1 specifies the schematic view of moving point heat source in 'x', 'y' and 'z' are the spatial terms with three mutually perpendicular direction (refer Fig. 1).

III. Experimental Work

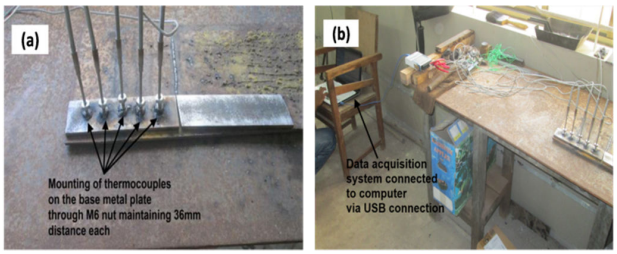

Fig. 2 Experimental images of measurement of thermal history in SMAW: (a) Mounting of thermocouples and (b) Data acquisition system connected to the thermocouple

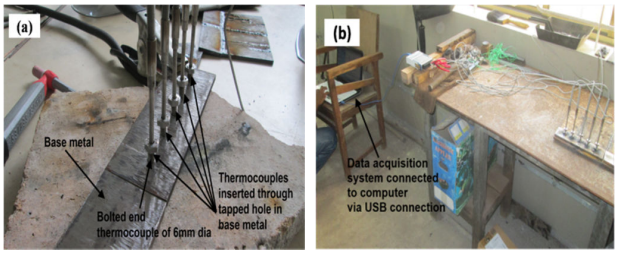

Fig. 3 Experimental images of measurement of thermal history in GTAW: (a) Mounting of thermocouples and (b) Data acquisition system connected to the thermocouple

TABLE I
Thermophysical Properties of AISI 1020 [24]

Quantity	Symbol	Value/Range
Density	ρ (kg/m^3)	7860
Thermal expansion coefficient	β (/°C)	11.7
Thermal conductivity	k (W/m-°C)	50
Specific heat	C_P (kJ/kg-°C)	0.465
Melting point	T_m (°C)	1450
Thermal diffusivity	α (m^2/s)	13.74
Emissivity	ε	0.4

TABLE II
Specifications of Experimental Set Up of SMAW and GTAW

Base metal	Size: 180×60×6 mm, Material: AISI 1020, Shape: Rectangular
Data acquisition system (DAQ)	NI 9213, 16 channel, 24-bit thermocouple unit, CAT II, Ch. to Earth isolation
SMAW welding Transformer	Oil cooled, 12KVA, 3ϕ, Primary-40V, 20/20/40 Amps, Secondary- 20/20/40 Amps, Secondary-20/40-8620/40-86
GTAW inverter	Welding amperage range: $3-350$A, Rated output: 250A at 30V, 100% Duty cycle, Maximum open circuit voltage: 75 DC
Filler metal	Copper coated triple de-oxidized mild steel rod
Inert gas used in GTAW	Argon
Thermocouple	K-Type

Experimental work has been conducted to predict the temperature distribution from the fusion line towards the longitudinal direction of the welded joint. As depicted in Figs. 2 (a) and 3 (a), five K-type thermocouples have been inserted on the surface of the welded plate maintaining 36 mm distance each, up to half of the thickness of the plate. The tapped holes are prepared (6mm diameter) on the surface of the plate and

thermocouples are mounted on these holes through M6 nut placed at the end of each wires to prevent any kind of ambient disturbance as it may cause heat loss and error of temperature measurement. The rear end of the thermocouple wires are connected with the Data acquisition system (DAQ), which in turn connected (refer Figs. 2 (b) and 3 (b)) with the LABVIEW software to estimate the signals provided by the wires during movement of heat source with the help of suitable programming. Table III denotes the experimental process parameters used for both SMAW and GTAW.

TABLE III
EXPERIMENTAL PROCESS PARAMETERS OF SMAW AND GTAW

Quantity	Symbol	Value/Range
Input current	I (A)	130
Input voltage	V (V)	40
Time of completing single pass	t (s)	70
Welding velocity	v (mm/s)	0.857
Heat transfer efficiency	η (%)	85
Heat input	H_{net} (J/mm)	5158
Radius of GTAW heat flux	R_a (mm)	3

IV. RESULTS AND DISCUSSION

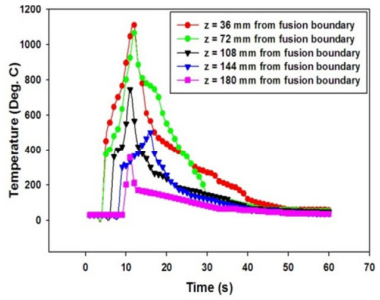

Fig. 4 Experimental temperature distribution of SMAW at I = 130 A from fusion boundary along the longitudinal direction

Fig. 4 demonstrates the experimental temperature distribution along the longitudinal direction from the fusion boundary for SMAW in which the peak temperature has been found 1115ºC at z = 36 mm (nearest region of weld pool) and it is very clear that formation of heating cycle is very rapid while cooling cycle is very gradual. As the distance increases along the longitudinal direction from the weld pool the temperature peak also becomes less. In addition, it has observed that higher temperature (in the range of 800ºC-1100ºC) has found in the domain of z = 36 mm – 72 mm. The reason is development of heat affected zone (HAZ). In case of GTAW, peak temperature is 1190ºC and it is higher than SMAW due to keyhole structure formation of moving point heat source. The intense beam of heat flow from tungsten torch with the environment of argon gas carries more heat than SMAW electrode. The tungsten material has unique quality of creating higher temperature in inert gas environment higher than its melting point. We have pointed out the thermal history within the time duration of 60s. In addition, the propagation of heat is faster in case of GTAW than SMAW. Both Figs. 4 and 5 pointed out the transient behaviour of experimental thermal history. These results can be well validated by the research work carried out by [25].

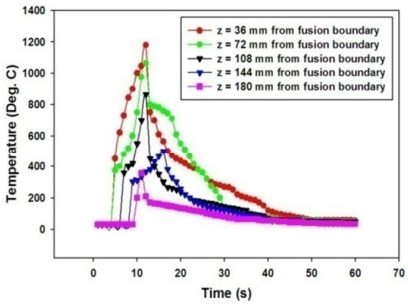

Fig. 5 Experimental temperature distribution of GTAW at I = 130 A from fusion boundary along the longitudinal direction

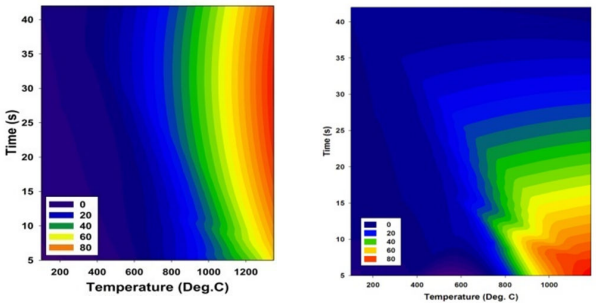

(a) (b)

Fig. 6 Propagation of cooling rate along the longitudinal direction from the fusion boundary at z = 36 mm (a) SMAW and (b) GTAW

Estimation of cooling rate is one of the most important factors as strength of the joint solely dependent on it and also it causes the development of several phases at welded region and it is in turn related with the quality of the joint. In present research work Adam's 2-dimensional equation (refer (1)) has been implemented to predict the cooling rate by implementing experimental temperatures keeping other thermophysical properties and experimental process parameters (refer Tables I and III) constant. From Fig. 6, it is evident that contour curve of cooling rate is varying gradually for SMAW while it is very much random in case of GTAW due to high peak temperature. The momentum exchange in liquid-solid interface is rapid due to high temperature and thus near the HAZ region, cooling rate deviation is experienced. Poorhaydari et al. [11] has Implemented Adam's equation for predicting cooling rate of different plate thickness and current research work shows contour curve generation which can be considered as modified result of application of Adam's 2-dimensional equation.

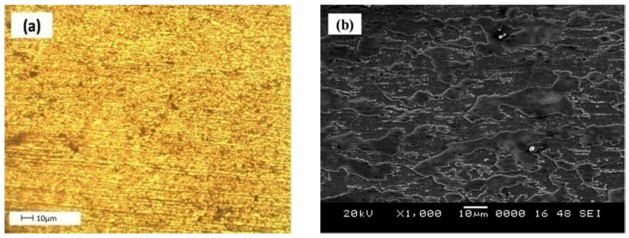

Fig. 7 Microstructural morphology of base metal of welded joint by SMAW (a) Optical micrograph (OM) and (b) Scanning electron micrograph (SEM)

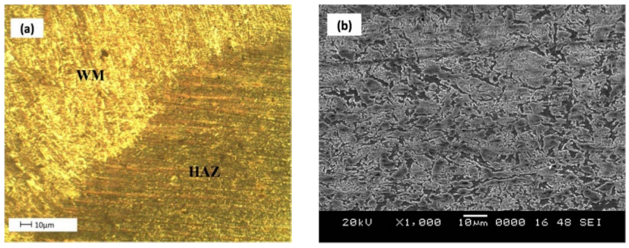

Fig. 8 Microstructural morphology of heat affected zone of welded joint by SMAW (a) Optical micrograph (OM) and (b) Scanning electron micrograph (SEM)

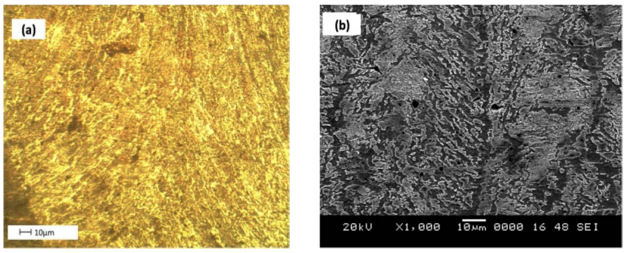

Fig. 9 Microstructural morphology of weld metal of welded joint by SMAW (a) Optical micrograph (OM) and (b) Scanning electron micrograph (SEM)

Fig. 7 depicts the microstructural analysis of base metal which consists of elongated grains termed as martensite. Also the SEM micrograph as depicted in Fig. 7 (b) has indicated the large globular structure in the vicinity of ferrite region and this also signifies the phenomena of rapid cooling. As heat input in this case is maximum compared to other three heat inputs, heat propagation is more from the weld pool towards the base metal is rapid and results as martensite. It means base metal is hard compared to other regions but brittle in structure. The weld metal as shown in Fig. 9 (a), is of interdendritic segregation of continuous orientation and the long black lamellas (refer Fig. 9 (b)) with white strips shows the fully transformed pearlite phase from austenite. This kind of pearlite is coarse in nature and shows hardness greater hardness compared with other pearlite formed in low heat inputs due to its large band of colonies. The segregation took place due to rapid cooling after high heat input. Comparison of HAZ region in other lower heat inputs in Fig. 8 (a) shows more compact fine pearlite with less colonial gap and continuous segregation of transformed fine pearlite. As the black spots appear less in Fig. 8 (b), it is the indication of less cementite (% in mass) presents in the phase and this in turn increases the hardness of the region with sufficient ductility.

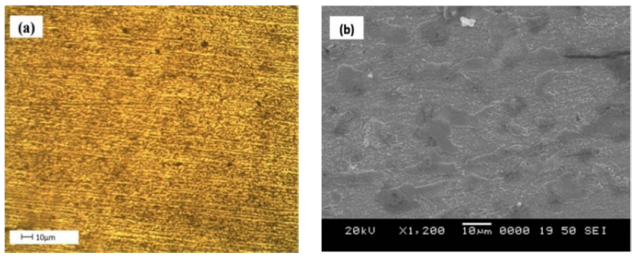

Fig. 10 Microstructural morphology of base metal of welded joint by GTAW (a) Optical micrograph (OM) and (b) Scanning electron micrograph (SEM)

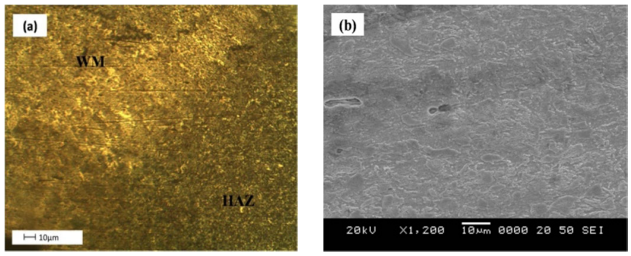

Fig. 11 Microstructural morphology of heat affected zone of welded joint by GTAW (a) Optical micrograph (OM) and (b) Scanning electron micrograph (SEM)

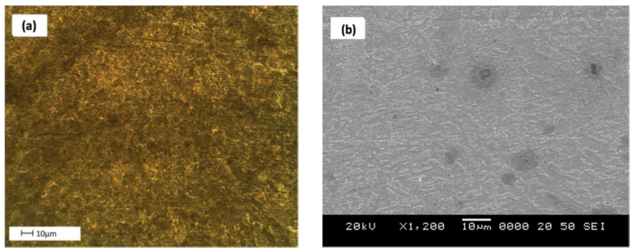

Fig. 12 Microstructural morphology of weld metal of welded joint by GTAW (a) Optical micrograph (OM) and (b) Scanning electron micrograph (SEM)

The grain structures as shown in Fig. 10 (a), is base metal region of GTAW 0.2% C steel at I = 130 A. This phase is also upper bainite but with transforming growth of pearlite. As the white thin lamella like structures are not as clear as shown in Fig. 10 (b). Thus the transformation phase has just started for pearlite. Also very small tiny particles of white colour have been found on the surface of base metal. The weld metal region as depicted in Fig. 12 (a), grains are in the form of interdendritic segregation with non-regular manner. Also from Fig. 12 (b), it has found that the bands of white lamellar are thin and black spots are less i.e. the volume fraction of cementite is less. Thus, it is a fine pearlite with high hardness. The black spherical spots are carbide precipitation formed due to flow of argon gas during the time of welding. According to Fig. 11 (b), in HAZ region shows partially similar grain orientation as compared to weld metal. However, the grains

are of bigger sizes (white spots) and they are non-uniformly placed on the surface of HAZ. Thus this phase can be termed as partially transformed fine pearlite with less cementite and hardness will be less than the phase appeared in weld metal.

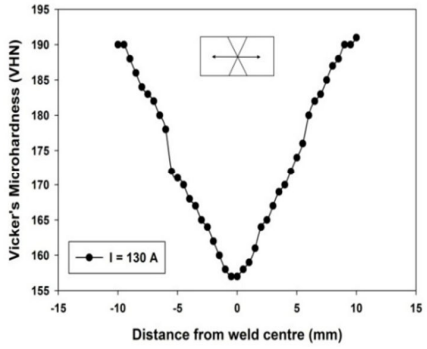

Fig. 13 Microhardness profile at different points of SMAW joint at I = 130 A

For the input current, I = 130 A, represented in Fig. 13, large band of colonial coarse pearlite in weld metal indicates highest hardness of 158-160 VHN among the other three heat inputs as discussed earlier. Also due to compact segregated structure of fine pearlite appears in HAZ, addresses hardness of 162-174 VHN. Whereas base metal shows formation of martensite and this phase has highest hardness among other phases of 178-190 VHN. Also it is evident that near the HAZ zone, base metal possesses higher hardness due to transformation of globular shaped grain boundaries.

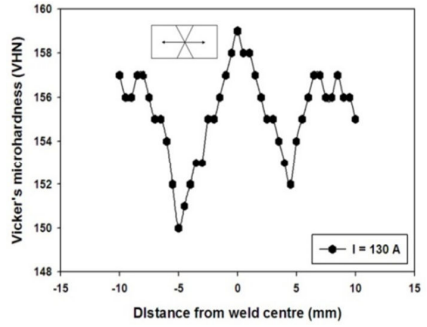

Fig. 14 Microhardness profile at different points of GTAW joint at I = 130 A

In case of I = 130 A (as shown in Fig. 14) fine pearlite has been observed in the weld metal region and it calculated the hardness of 159 VHN. This is possible due to less volume fraction of cementite. The gradual fall of hardness in HAZ region is due to formation of partially transformed fine pearlite region and it has lower hardness, 151 VHN. As per results and discussion (refer Fig. 10 (b)), the base metal region is upper bainite with starting zone of pearlite transformation, a very slow and gradual increment of hardness has been estimated up to 157 VHN after HAZ along the base metal region.

V. Conclusion

From the present research work, the following concluding remarks can be summarized:

(a) Experimental temperature history consists of fast heating cycle and slow (gradual) cooling cycle. Weld pool takes fraction of second to solidify from liquid to solid phase followed by slow cooling process. In case of GTAW, around 75℃ higher peak temperature has been observed compared to SMAW.

(b) Cooling rate based on Adam's 2-dimensional equation, strictly follows the experimental thermal profile and justifies the results and justification provided by [11].

(c) The microstructure morphology and microhardness investigation indicate that welded joint of AISI 1020 is suitable for SMAW in the range of I = 130 A as the higher hardness has been observed compared to GTAW. But formation of martensite in the interface boundary of HAZ-base metal weakens the joint due to high brittleness. In case of GTAW, though microhardness varied but range of hardness is less (150 VHN – 160 VHN). Thus from the point of view of ductility, GTAW provides more durability than SMAW.

Acknowledgment

The authors would like to thank Dr. Narendranath S., Professor of Department of Mechanical Engineering, National Institute of Technology Karnataka, Surathkal, India for his extensive help and motivation to carry out metallurgical analysis of welded joints.

References

[1] J. A. Goldak and M. Akhlaghi, *Computational welding mechanics*. Spring Street, New York 100013, USA: Springer Science+Business Media Inc, 2005.

[2] Rosenthal D., "The theory of moving sources of heat and its applications to metal treatments", Trans. ASME, 1946, Vol. 68, pp. 849-865.

[3] Pavelic V. Et al., "Experimental and computed temperatures histories in gas tungsten arc welding of thin plates, Welding Journal Research Supplement", 1969, Vol. 48, pp. 2952-305s.

[4] C. L. Tsai and C. A. Hou, "Theoretical analysis of weld pool behaviour in the pulsed current GTAW process", Journal of Heat Transfer, 1988, vol. 110, pp. 160-165.

[5] Jones BK, Emery AF and Marburger J. An analytical and experimental study of the effects of welding parameters in fusion welds, Welding J., 1993, Vol. 72, No. 2, pp 5 IS-59s.

[6] Goldak J. A. et al., "Thermal stress analysis in solids near the liquid region in the weld: Mathematical modeling of weld phenomena", The Institute of Materials, 1997, pp. 543 -570.

[7] Little G. H. and Kamtekar A. G., "The effect of thermal properties and weld efficiency on transient temperatures in welding", Computers and Structures, 1998, vol. 68, pp. 157 - 165.

[8] Komanduri R. and Hou Z. B., "Thermal analysis of arc welding process: Part I. General solutions", Metallurgical and Materials Transactions B, 2000, vol. 31B, pp. 1353 - 1370.

[9] Komanduri R. and Hou Z. B., "Thermal analysis of arc welding process: Part II. Effect of Thermophysical Properties with Temperature", Metallurgical and Materials Transactions B, 2001, vol. 33B, pp. 483 - 499.

[10] Zhu X. K. and Chao Y. J., "Effect of temperature dependent material properties on welding simulation", Computers and Structures, 2002, vol. 80, pp. 967 - 976.

[11] Poorhaydari K. Et al., "Estimation of cooling rate in the welding of plates with intermediate thickness", Welding Journal, 2005, pp. 149s - 155s.

[12] Mousavi Akbari S. A. A. and Miresmaeili R., "Experimental and numerical analyses of residual stress distributions in TIG welding process for 304L stainless steel", Journal of Material Processing Technology, 2008, vol. 208, pp. 383 - 394.
[13] Del Coz Diaz J. J. Et al., "Comparative analysis of TIG welding distortions between austenitic and duplex stainless steels by FEM", Applied Thermal Engineering, 2010, vol. 30, pp. 2448 - 2459.
[14] Pathak C. S. Et al., "Analysis of thermal cycle during multipass arc welding", Welding Journal, 2012, vol. 91, pp. 149s - 154s.
[15] Ravisankar A. et al., "Influence of welding speed and power on residual stress during gas tungsten arc welding of thin sections with constant heat input: A study using numerical simulation and experimental validation", J. of Manufacturing Process, 2014, vol. 16, pp. 200 - 211.
[16] Alireza B. et al., "Computational analysis of the effect of welding parameters on energy consumption in GTA welding process", International Journal of Mechanical Sciences, 2015, vol. 93, pp. 111-119.
[17] Mohandas T et al., "A comparative evaluation of gas tungsten and shielded metal arc welds of a "ferritic" stainless steel", Journal of Materials Processing Technology, 1999, vol. 94, pp. 133-140.
[18] Datta R et al., "Weldability characteristics of shielded metal arc welded high strength quenched and tempered plates", Journal of Material Engineering and Performance, 2002, vol. 11 (1), pp. 5-10.
[19] Ahmet Durgutlu, "Experimental investigation of the effect of hydrogen in argon as a shielding gas on TIG welding of austenitic stainless steel", Materials and Design, 2004, vol. 25, pp. 19-23.
[20] Bala Srinivasan P. et al., "Microstructure and corrosion behaviour of shielded metal arc welded dissimilar joints comprising duplex stainless steel and low alloy steel", Journal of Material Engineering and Performance, 2006, vol. 22, pp. 758-764.
[21] Magudeeswaran G. et al., "Effect of welding processes and consumables on high cycle fatigue life of high strength, quenched and tempered steel joints", Materials and Design, 2008, vol. 29, pp. 1821-1827.
[22] Moeinifar S. et al., "Influence of peak temperature during simulation and real thermal cycles on microstructure and fracture properties of the reheated zones", Materials and Design, 2010, vol. 31, pp. 2948-2955.
[23] Chuaiphan Wichan and Srijaroenpramong Loeshpahn, "Effect of welding speed on microstructures, mechanical properties and corrosion behaviour of GTA welded AISI 201 stainless steel sheets", Journal of Materials Processing Technology, 2014, vol. 214, pp. 402-408.
[24] Dieter George E., "Mechanical Metallurgy", McGraw Hill, 3rd ed. Pp 75-77.
[25] Goncalves C V, Carvalho S R and Guimaraes G, "Application of Optimization Techniques and the Enthalpy Method to Solve a 3-D Inverse Problem During a TIG Welding Process", Applied Thermal Engineering, 2010, vol. 30, pp. 2396-2402.